Nanoscale

Accepted Manuscript

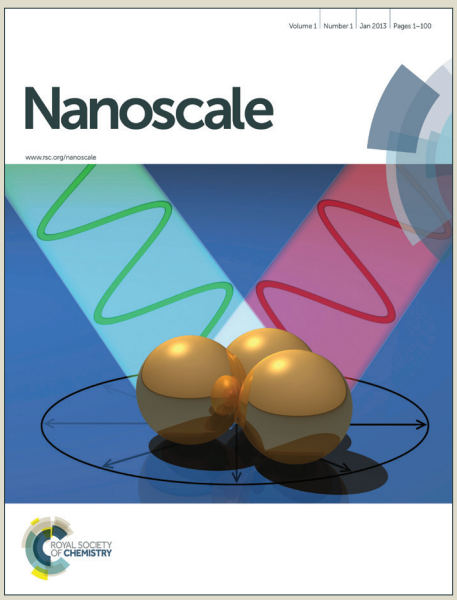

ROYAL SOCIETY OF CHEMISTRY

www.rsc.org/nanoscale

A safe and efficient hepatocyte-selective carrier system based on myristoylated preS1/21-47 domain of hepatitis B virus

Quan Zhang[a,1], Xuanmiao Zhang[a,1], Tijia Chen[a], Xinyi Wang[a], Yao Fu[a], Yun Jin[b,*], Xun Sun[a], Tao Gong[a,*], Zhirong Zhang[a]

1 Contributed equally to this work.

a Key Laboratory of Drug Targeting and Drug Delivery Systems, Ministry of Education, West China School of Pharmacy, Sichuan University, Chengdu 610041,China

b National Institute of Drug Clinical Trial, Sichuan Academy of Medical Sciences & Sichuan Provincial People's Hospital, Chengdu 610072, China

*Corresponding author.

Tao Gong

Key Laboratory of Drug Targeting and Drug Delivery Systems, West China School of Pharmacy, Sichuan University, No. 17, Section 3, RenminSouthRoad, Chengdu, Sichuan 610041, China

Tel./fax: + 86 28 8551615. E-mail: gongtaoy@126.com

Yun Jin

National Institute of Drug Clinical Trial, Sichuan Academy of Medical Sciences & Sichuan Provincial People's Hospital, No. 32 W. Sec 2, 1st Ring road, Chengdu, Sichuan Province 610072, PR China.

Tel./fax: + 86 28 87393401. E-mail: jy1356@126.com

Abstract

A safe and efficient liver targeted PEGylated liposome (PEG-Lip) based on N-terminal myristoylated preS1/21-47 (preS1/21-47^{myr}) of hepatitis B virus was successfully developed. The study aimed to elucidate the cellular uptake mechanism of preS1/21-47^{myr} modified PEG-Lip (preS1/21-47^{myr}-PEG-Lip) in hepatogenic cells and the distribution behavior of preS1/21-47^{myr}-PEG-Lip in Vr:CD1(ICR) mice. The cellular uptake results showed preS1/21-47^{myr}-PEG-Lip were effectively uptaken by hepatogenic cells (including primary hepatocytes and liver tumor cells) through a receptor-mediated endocytosis pathway compared with non-hepatogenic cells. After systemic administration to H22 hepatoma-bearing mice, preS1/21-47^{myr}-PEG-Lip showed significant liver-specific delivery and an increase in the distribution of preS1/21-47^{myr}-PEG-Lip in hepatic tumor. Furthermore, the antitumor effect of preS1/21-47^{myr}-PEG-Lip loaded with paclitaxel (PTX) was remarkably stronger than that of PTX injection and PTX loaded liposomes (including common liposomes and PEG-Lip). In safety evaluation, no acute systemic toxicity and immunotoxicity were observed after intravenous injection of preS1/21-47^{myr}-PEG-Lip. No liver toxicity was observed despite the dramatic increase of preS1/21-47^{myr}-PEG-Lip in liver. Taken together, preS1/21-47^{myr}-PEG-Lip represents a promising carrier system for targeted liver disease therapy and imaging.

Keywords: PreS1/21-47^{myr}, Liver-targeted delivery system, PEGylated liposomes, Hepatogenic cells, Differentiation

1. Introduction

Liver is one of most important organs in the human body which plays a critical role in the metabolism and excretion of diverse endogenous and exogenous compounds. Liver diseases, such as virus infections, liver cirrhosis, liver injury and hepatocellular carcinoma, continuously challenge the human health due to the serious lack of effective treatment options [1]. One major drawback for the standard therapy of liver diseases is the inability of delivering sufficient drugs specifically to the liver [2]. Also, major side effects for tumor chemotherapy are tissue/organ-dependent, and thus it is more desirable to selectively deliver the therapeutics to the target sites rather than increase the dosage for achieving the therapeutic drug concentration at the target sites[3].

In the past decades, various strategies have been developed to achieve targeted delivery of therapeutic agents to the liver. The nanoparticulate delivery systems, particularly liposomes and polymeric nanoparticles, were extensively studied as liver-specific drug carriers based on the size-dependent passive targeting strategy. After intravenous injection, nanoparticulate carriers are easily phagocytosed within seconds or minutes by the reticuloendothelial system (RES), including Kupffer cells of the liver and macrophages of the spleen [4, 5]. However, drugs were shown to mainly distribute in the liver Kupffer cells and not in the hepatic parenchymal cells which were the main disease cells [2]. To circumvent such disadvantages, liver targeting ligands, particularly galactose [6, 7], mannose [8, 9], glycyrrhetinic acid [10, 11] and apolipoprotein [12] were adopted to achieve active targetability to liver. However, the application of these ligand-based carriers is severely limited by the following disadvantages [12-16]: poor specificity, impaired binding affinity after conjugation,

potential immunogenicity and high cost. Therefore, seeking alternative approaches remains a great challenge for developing liver-targeted drug delivery systems.

In addition to nanoparticulate carriers and liver targeting ligands based delivery systems, the viral-mediated delivery systems could also deliver therapeutics to the liver with high efficiency. Many viruses such as adenoviruses, hemagglutinating virus of Japan, retrovirus, lentiviral vectors and human hepatitis B virus (HBV) have been used to deliver drugs or genes to the liver successfully [2, 17]. Among these viruses, HBV displays a pronounced liver tropism and specifically targets to the liver. Extensive studies have been conducted using HBV as a carrier system[18-20] and its surface envelope proteins as a delivery system[17, 21, 22] or targeting moiety [23, 24]. However, their application is severely constrained by the safety of viral carriers[25] and the strong immunogenicity of extrinsic proteins [26, 27].

The envelope protein of HBV consists of large (L), middle (M), and small (S) proteins [28]. Furthermore, the L protein have a further N-terminal extension with 107, 117, or 118 amino acids (genotype-dependent) termed preS1 which is N-terminally myristoylated and plays an pivotal role in HBV entry into liver cells (Fig. 1)[29-32]. Petersen et al[33] found that synthetic N-terminally myristoylated preS1/2-48 (preS1/2-48^{myr}) could block HBV infection *in vitro* and *in vivo* with high efficacy and specificity. Especially, preS1/2-48^{myr} was proven to show good hepatotropism which was mediated by the special receptor recognition in the liver [34] and preS1/2-48^{myr} was found a good ligand for liver targeted delivery system and showed no immunotoxicity in our previous study [35]. However, the preS1/2-48^{myr} could not mediates specific binding to the hepatocellular carcinoma cells such as HuH7 and HepG2 cells [36]. Further studies showed that the preS1(21-47) region, a shorter amino acid sequence than preS1/2-48, may be one of the vital peptide sequence to mediate interaction of

HBV with hepatic cells such as HepG2 cells [37-39]. Based on this, Masaharu et al[40] prepared nanoscale protein cages with a ligand composed of preS1 aa21-47 peptide of HBV by genetic engineering techniques. The protein nanocages showed significantly higher specificity to human hepatocyte cancer cell lines than other non-liver cell lines *in vitro*. However, the targeting efficiency and immunogenicity *in vivo* are not studied.

In this study, the N-terminally myristoylated preS1 aa21-47 peptide (preS1/21-47^{myr}) (Fig. 1) was designed and synthesized via solid phase peptide synthesis for the N-terminal myristoylated modification of HBV which is critical to the efficient infection and the functional affinity of preS1 peptide with hepatocytes [26, 31, 41]. As the targeting ligand, preS1/21-47^{myr} was utilized to modify PEGylated liposomes. We here followed the question of whether the drug delivery system had the potential to be a novel, efficient and safe liver-targeting drug delivery system. Furthermore, the targeting efficiency and toxicity of this drug delivery system were systematically studied.

2. Experimental section

2.1 Materials and animals

The preS1/21-47^{myr} with or without a C-terminal cysteine (myristic acid-PLGFF PDHQL DPAFG ANSNN PDWDF NP-Cys) was synthesized according to the solid phase peptide synthesis by Kaijie Biopharmaceutical Co., Ltd. (Chengdu, China). Mal-PEG$_{2000}$-DSPE was obtained from Laysan Bio., Inc. (USA). Lipoid S100 and mPEG$_{2000}$-DSPE were purchased from Lipoid Co., Ltd (Ludwigshafen, Germany) and cholesterol was purchased from Kelong Chemical Company (Chengdu, China). Did

(1,1'-dioctadecyl-3,3,3',3'-tetramethyl indodicarbocyanine, 4-chlorobenzenesulfonate salt) was purchased from Biotium (Hayward, USA). Paclitaxel (PTX) injection was purchased form Sichuan tai chi pharmaceutical co., Ltd. (Chengdu, China) and PTX from Shanghai Biochempartner Co., Ltd. (Shanghai, China). 3-(4,5-Dimethyl-2-thiazolyl)-2,5-diphenyl-2H-tetrazolium bromide (MTT), lipopolysaccharides from Escherichia coli 055:B5 (LPS) and 4,6-Diamidino-2-phenylindole (DAPI) were obtained from Sigma-Aldrich Co. LLC (USA). RPMI1640 media and fetal bovine serum (FBS) were purchased from Thermo Fisher Scientific, Inc. (USA). All other reagents were of analytical grade or better.

Vr:CD1 (ICR) mice with ages of 7-8 weeks were purchased from Dashuo experimental animal, Inc. (Chengdu, China). All animal experiments were performed in compliance with the guidelines of the Care and Use of Laboratory Animals and approved by the Experiment Animal Administrative Committee of Sichuan University.

2.2 Preparation and characterization of liposomes

2.2.1 Preparation

Liposomes were prepared by the standard thin-film hydration method as described previously [42] with minor modifications. Briefly, S100, cholesterol, $mPEG_{2000}$-DSPE and Mal-PEG_{2000}-DSPE (molar ratio = 22.5:15:1.7:0.3) were dissolved in dichloromethane. After the organic solvent was removed by rotary evaporation, the thin film was hydrated at 37 ℃ for 1h in 5% glucose solution. The obtained multilamellar vesicles were further intermittently sonicated by a probe sonicator at 180 W for 1.5 min to form the maleimide derivatized PEGylated liposomes (Mal-PEG-Lip). The conventional PEGylated liposomes (PEG-Lip) were prepared as

described above with the Mal- PEG_{2000}-DSPE being replaced by $mPEG_{2000}$-DSPE. The common liposomes (cLip) consisted of only S100 and cholesterol with a molar ratio of 2:1 were also prepared by the standard thin-film hydration method. Did-labeled liposomes were prepared with Did added to the lipid organic solution prior to the solvent evaporation.

Mal-PEG-Lip modified with preS1/21-47^{myr} (preS1/21-47^{myr}-PEG-Lip) was prepared by maleimide-thiol coupling reaction in HEPES buffer (pH 7.4) at room temperature for 30 min. The thiol of preS1/21-47^{myr}-Cys was reacted with maleimide of the Mal-PEG-Lip at 1.5:1 molar ratio. The unconjugated peptide was removed by passing through a Sephadex G75 column.

PTX loaded liopsomes were prepared as Did labled liposomes with Did being replaced by PTX.

2.2.2 Characterization

2.2.2.1 Particle size, zeta potential and morphology of liposomes

The particle size and zeta potential of liposomes were determined by dynamic light scattering (DLS) using Zetasizer Nano ZS90 instrument (Malvern, UK). All the measurements of particles size were made with liposome formulations diluted by 20 fold in 5% glucose solution at room temperature and measured at a light scattering angle of 90 degree with the intensity-weighted mode. The liposomes were directly measured for the zeta potential without further dilution.

The morphology of liposomes was observed by transmission electron microscopy (TEM) (H-600, Hitachi, Japan). For the analysis of TEM, the liposome formulation was adjusted to about 1.0 mg/mL of lipid and stained with 2% (w/w) phosphotungstic acid (PTA).

2.2.2.2 Encapsulation efficiency and *in vitro* release profile of PTX loaded liposomes

The entrapment efficiency of PTX loaded liposomes was investigated through the ultrafiltration method [35]. Briefly, 0.2 mL of PTX loaded liposomes were disrupted in methanol and sonicated for 10 min, then suspension was centrifuged to collect supernatant and the PTX was quantitatively analyzed by high performance liquid chromatography (HPLC) as the total added amount of PTX (W_{total}). In addition, another 0.2 mL PTX loaded liposomes was ultrafiltrated and the filtrate was collected to analyze the free PTX (W_{free}) by HPLC. The entrapment efficiency was calculated using the following formula:

$$\text{Entrapment efficiency} = (W_{total} - W_{free}) / W_{total} \times 100\%$$

The *in vitro* release profile of PTX loaded liposomes was investigated as described as follows. 1 mL of PTX-loaded liposomes or free PTX solution was transferred into dialysis bags (molecular weight cut-off 10000 Da) respectively. Then the dialysis bags were immersed in 50 mL PBS (pH 7.4) containing 0.05% (v/v) Tween 80 and placed in a shaker with a speed of 100 rpm at 37 ℃. At predetermined time intervals, 0.5 mL of release medium was collected and replaced with 0.5 mL fresh medium. Then the samples were diluted with methanol and PTX was quantified by HPLC.

2.2.3 Validation of the conjugation of preS1/21-47^{myr} to Mal-PEG2000-DSPE

2.2.3.1 Tricine-SDS-PAGE

The preS1/21-47^{myr}-Cys was dissolved in the Hepes buffer (1M, pH 7.4), and then the buffer was added into the Mal-PEG_{2000}-DSPE in 5% glucose solution. After 30 min, the reaction solution was subjected to the tricine-sodium

dodecylsulfate-polyacrylamide (tricine-SDS-PAGE) electrophoresis with 16% SDS-PAGE [43].

2.2.3.2 Quantification of the preS1/21-47^{myr} on the liposomes

To determine the amount of the preS1/21-47^{myr} conjugated to the liposomes, the Micro BCA method with simple modification [44] was adopted and the absorbance was measured at 562 nm using a spectrophotometer (Thermo Scientific Varioskan Flash, Thermo Fisher Scientific, USA).

2.2.4 Colloidal stability of liposomes

2.2.4.1 Storage stability

Storage stability of the prepared liposomes was evaluated by storing the liposome formulations at 4 ℃ for 4 weeks and the particle size was monitored by the DLS throughout the period.

2.2.4.2 Serum stability

To evaluate the serum stability of liposomes, the variation of particle size of liposomes was assayed in the presence of FBS and monitored by the DLS [42]. In brief, liposome solutions were mixed with equal volume of FBS and incubated in a water bath at 37 ℃ with gentle shaking. At predetermined time points, 0.2 mL of the sample was diluted by 10 fold in 5% glucose solution and the particle size of the liposomes was measured by the DLS.

2.3 Cell culture

2.3.1 Cell isolation

Primary hepatocytes were isolated from ICR mice by the method as described previously with minor modifications [45]. In brief, liver tissues were perfused with

ethylene glycol tetraacetic acid (EGTA) perfusion buffer (consisting of 0.5% Glucose, 25 mM HEPES, 2 mM EGTA in PBS, pH 7.4, sterile filtered, pre-heated to 37 ℃) for 5 min until the liver turned to be khaki color. Then the liver tissues were perfused with collagenase perfusion buffer (consisting of 25 mM HEPES, 3 mM $CaCl_2$, 3 mg/ml collagenase type IV in plain DMEM medium, pH 7.4, sterile filtered, pre-heated to 37 ℃) for 5 min. After perfusion, the liver tissues were collected and dispersed in DMEM medium with sterile tweezers. After filtered through 100 μm nylon mesh, the cell suspension was centrifuged at 50 × g for 3 min at 4 ℃. To isolate the hepatocytes from total cells, the cell pellet was washed and centrifuged at 50 × g for 3 min two times in DMEM medium, and the cells at the bottom were the purified hepatocytes. After the viability was checked by trypan blue exclusion, hepatocytes were plated in cell culture plates at the required density and incubated in DMEM medium supplemented with 10% FBS. Cells were incubated at 5% CO_2 and 37 ℃.

2.3.2 Cell differentiation

A549 cells and HepG2 cells were incubated as monolayer cultures in RMPI 1640 medium supplemented with 10% FBS at 5% CO_2 and 37 ℃. To induce differentiation [36, 46], cells were cultured in the medium with 1% dimethylsulfoxide (DMSO) for 5 days.

2.4 Assessment of liposomes uptake *in vitro*

2.4.1 Flow cytometry

The cellular uptake of Did-labeled liposomes was evaluated using a flow cytometer (FCM, CytomicsTM FC 500, Beckman Coulter, USA) in accordance with the protocol of previous report [47]. In brief, cells were seeded in 12-well plates at a density of 1×10^5 cells/mL and incubated for 24 h at 37 ℃. Then, the medium was

replaced with 1 mL of fresh medium containing mPEG-Lip, preS1/21-47^{myr}-PEG-Lip or cLip with an equivalent concentration of Did (400 ng/mL), and the cells were incubated for 1 h at 37 ℃. The cells were washed thrice with cold PBS, then trypsinized and pelleted by centrifugation. The cell pellets were resuspended in 0.3 mL of PBS and measured by FCM.

In the competitive inhibition assay, cells were pre-incubated with 25 μg/mL of free preS1/21-47^{myr} for 1 h, and afterwards the culture medium was replaced with fresh medium containing Did-labeled liposomes. After 1 h, the cells were examined by FCM.

2.4.2 Confocal laser scanning microscopy

For microscopic observation, cells were seeded on cover slips in 12-well plates at a density of 1 × 10^4 cells/mL and incubated for 24 h at 37 ℃. Then, the medium was replaced with 1 mL of fresh medium containing mPEG-Lip, preS1/21-47^{myr}-PEG-Lip or cLip with an equivalent concentration of Did (400 ng/mL) and allowed for further incubation of 1 h. Then the cells were washed thrice with cold PBS and fixed in 4% paraformaldehyde at room temperature for 10 min, following by nuclei staining with DAPI (1 μg/mL) for 5 min. Finally, cells were observed using a confocal laser scanning microscopy (FV1000, Olympus, USA).

2.5 Mechanism of cellular uptake

To study the mechanism of liposomes internalization, the relative cellular uptake of liposomes with 400 ng/mL of Did was measured in HepG2 cells, differentiated HepG2 cells and primary hepatocytes with selective inhibitors of different endocytosis pathways. Specifically, Cells were seeded in 12-well plate and incubated as described in the previous section. Cells were pre-incubated for 30 min with plain

medium containing (inhibitors) sodium azide (0.1%, w/v), filipin (10 μg/mL), colchicine (1 mM), and chlorpromazine (20 μg/mL). The medium was then discarded and the cells were washed thrice with PBS, and incubated for another 2 h with Did (400 ng/mL) containing liposomes. After that, cells were washed thrice with ice-cold PBS, trypsinized and pelleted by centrifugation, and then resuspended in 0.3 mL of PBS for FCM analysis. The relative uptake of liposomes was expressed as the ratio of the florescence reading for the inhibitor pre-treated cells to that for the corresponding non-treated cells.

2.6 *In vitro* cytotoxicity

The cell cytotoxicity of liposmes in the study was assessed on HepG2, differentiated HepG2 and primary hepatocytes by MTT viability assay [48]. In brief, cells were seeded in 96-well plates at 1×10^4 cells/well and incubated for 24 h. After that, the cells were exposed to blank liposomes (31.25 - 1000 μg/mL of lipid) in fresh medium for 24 h. Subsequently, the medium was replaced by 200 μL of MTT solution (0.5 mg/mL in fresh medium) and cells were further incubated for 4 h at 37 ℃. The medium was then discarded and the formazan crystals were dissolved in 200 μL of DMSO. The absorbance was measured at 570 nm by a microplate reader (Thermo Scientific Varioskan Flash, USA). Cell viability (%) was calculated according to the following formula: $(Abs_{test}\text{-}Abs_{blank}/Abs_{control}\text{-}Abs_{blank}) \times 100\%$, where Abs_{test} and $Abs_{control}$ represented the absorbance of cells treated with liopsomes and blank culture medium respectively, and Abs_{blank} was the absorbance of cells without treatment with MTT.

2.7 *In vivo* biodistribution study

The liver and liver tumor targetability of liposomes was investigated in a tumor-xenograft mouse model by acquiring the fluorescence of liver and liver tumor. To prepare the H22 tumor-xenografted mouse model, the male ICR mice were used and injected at the right axilla with a H22 cell suspension (1×10^6 cells in 0.2 mL). 2 weeks later, the liposomes were injected through tail vein at a dose of 150 μg Did/kg. 1 h after injection of liposomes, the mice were immediately executed and the intact major organs and tumors were collected and imaged with *in vivo* imaging system (Quick View 3000, Bio-Real, Austria). The fluorescence intensity of different organs and tumors was acquired to calculate the statistical differences by the semi-quantitative analysis of the *ex vivo* fluorescent images.

2.8 *In vivo* parenchymal hepatic cell targeting study

To study the distribution of liposomes in the parenchymal hepatic cells, Did-labeled liposomes were injected into ICR mice via tail vein at a dose of 150 μg Did/kg. 1 h after the injection, hepatocytes were isolated from liver and purified as described in previous section. The hepatocytes suspension was analyzed by FCM.

2.9 *In vivo* antitumor efficacy

H22 cells (1×10^6 cells per mouse) were inoculated subcutaneously to the ICR mice at the right axilla. On Day 7, mice were randomly divided into five groups. Each group contains 12 mice. PTX injection and different PTX liposomes were administered (5 mg/kg) via the tail vein once each at day 7, 10, 13 and 16. Normal saline was administrated via intravenous injection for the control group. Tumor was measured by a vernier calipers on alternate day and its volume (V) was calculated as the formula $0.5\ (a \times b^2)$ where "a" and "b" are the longest and shortest diameter of the

tumor, respectively [49]. The survival of the mice was recorded and presented by Kaplan-Meier plots.

2.10 *In vivo* toxicity studies

2.10.1 General toxicity

The general toxicity of liposomes in this study was examined in accordance with the literature with minor modifications [50]. Briefly, male ICR mice were fasted for 12 h before an intravenous injection of blank liposomes (150 μmol/kg) or saline and the injection was carried out once every two days for two consecutive weeks. The mice were weighed daily and sacrificed at 24 h after the last administration. The blood samples were collected for standard hematologic and biochemical analysis. For hematologic analysis, the blood samples were directly measured by automatic hematology analyzer (MEK-6318K, Nihon-kohden, Japan) for the amount of white blood cell count (WBC), red blood cell count (RBC), hematocrit, hemoglobin, lymphs, platelet count, mean corpuscular hemoglobin (MCH), mean corpuscular volume (MCV) and mean corpuscular hemoglobin concentration (MCHC). As for biochemical analysis, the blood samples collected were kept at 4 ℃ for 30 min and centrifuged at 4000 rpm for 10 min at 4 ℃. The supernatant (serum) was collected to being assayed using automatic biochemical analyzer (7020, Hitachi, Japan) for the level of glutamic-pyruvic transaminase (ALT), glutamic-oxalacetic transaminase (AST), alkaline phosphatase (ALP), blood urea nitrogen (BUN), creatinine (CREA), lactate dehydrogenase (LDH), total creatine kinase (CK), and total bilirubin. Organs including heart, liver, spleen, lung, kidney and brain were excised for histopathologic observation [51]. In brief, the organs were fixed with 4% paraformaldehyde for at least 48 h and then embedded in paraffin. The blocks were cut into 5 μm thickness and the tissue sections were stained with hematoxylin and eosin (H & E). The histological

sections were examined and photographed under light microscopy (Axiovert 40CFL, CarlCeiss, Germany).

2.10.2 Immunotoxicity

To investigate the immunogenicity of liposomes *in vivo*, the levels of interleukin-6 (IL-6) and interleukin-12 (IL-12) in serum were evaluated as previously reported [52]. In a nutshell, male ICR mice were intravenously injected with blank preS1/21-47^{myr}-PEG-Lip (150 μmol/kg), saline and LPS (2 mg/kg), respectively. 2 h after injection, blood samples were collected and serum samples were isolated to determine IL-6 and IL-12 levels by ELISA assay (R&D Systems, USA).

2.11 Statistical analysis

Statistical comparisons were performed using Student's *t*-test to evaluate statistical differences among groups. All data reported are expressed as mean ± SD (standard deviations). Data with $P < 0.05$ and $P < 0.01$ were considered to be statistically different and statistically significantly different, respectively.

3. Results and discussion

3.1 Preparation and characterization of liposomes

In this study, the preS1/21-47^{myr}-PEG-Lip was prepared through the water phase reaction method [53] by which the preS1/21-47^{myr}-Cys reacted with Mal-PEG-Lip and not the thin-film hydration method by which preS1/21-47^{myr}-conjugated PEG-DSPE was incorporated into the organic solution of lipids prior to the thin film formation. In the preliminary study, the preS1/21-47^{myr}-PEG-Lip prepared by the thin-film hydration method and the PEG-Lip modified by preS1/21-47 without N-terminal myristoyl through the water phase reaction method did not show satisfactory uptake by liver cells (data not shown). The results were inconsistent with the result of

literature [40] in which the nanoscale protein cage modified with preS1 aa21-47 peptide of HBV was fabricated by genetic engineering and showed excellent specificity for hepatic cell lines than other cell lines. This contradiction might be explained by that the N-terminal myristoylated modification was suggested to improve the functional affinity of preS1 peptide with hepatocytes [54] and the specific uptake of liposomes by the liver cells might require higher functional affinity of preS1 peptide with hepatocytes than that of the nanoscale protein cage. Moreover, it was also reported that the N-terminal myristoylated modification of preS1 peptide was essential for viral infectivity of HBV[31]. Based on these observations, the myristoyl acid residue in preS1/21-47^{myr} might be buried in the lipid bilayer of liposomes during the hydration process thus resulting in the poor performance of preS1/21-47^{myr}-PEG-Lip.

As shown in Fig. 2, maleimide-thiol addition reaction completed in about 30 min under gentle conditions. The amount of preS1/21-47^{myr} on the surface of liposomes was quantified by Micro BCA assay. The amount of modified preS1/21-47^{myr} was determined as approximately 13.47 ± 1.22 μg/μmol lipids.

Table 1 shows the hydrodynamic size and the zeta potentials of liposomes in 5% glucose solutions. The average particle size of PEGylated liposomes was about 120 nm and slightly increased after preS1/21-47^{myr} modification. Furthermore, the particle size of cLip was bigger than that of preS1/21-47^{myr}-PEG-Lip. As for the zeta potential, obtained liposomes displayed negative charges. The morphology of liposomes was observed by TEM. The prepared liposomes displayed uniform and near spherical shapes under TEM (Fig. 3A), and the diameter was in the nanometer range which was consistent with the DLS measurement. In addition, all of these parameters were not significantly affected by the PTX loading and the encapsulation efficiency of PTX

was more than 90% (Table 1), illustrating that PTX was well incorporated into the liposomes.

The *in vitro* release profiles of PTX loaded liposomes were presented in Fig. 3B. Compared with the rapid release of free PTX, all of PTX loaded liposomes showed the sustained release properties and there was no obvious burst release. In addition, the release of PTX from cLip was slightly quicker than that of PEG-Lip and preS1/21-47^{myr}-PEG-Lip but there were no significant differences between PEG-Lip and preS1/21-47^{myr}-PEG-Lip which indicated that the PEG chain might slow the drug release of cLip and the peptide modification showed little influence on the drug release profile of PEG-Lip.

Due to the fusion or aggregation of unstable liposomes during the preparation and/or storage process, the increase in particle size of liposomes was a typical phenomenon [55]. In this study, the storage stability of liposomes was evaluated by storing liposomes formulations at 4 ℃ for 4 weeks and by monitoring the variation of particle size using DLS. As shown in Fig. 4A, the PEGylated liposomes including preS1/21-47^{myr} modification showed a stable particle size over the storage period. However, cLip became bigger at four days and even there was some precipitate on the bottom of container after 1 week which could be attributed to the fusion and aggregation of liposomes. For cLip was only used as a control and swiftly used after being prepared, the stability condition of cLip was not investigated.

Opsonization (*i.e.* protein adsorption) can induce significant changes in the liposomal surface properties, which is likely to result in rapid clearance of liposomes from the blood and affects their *in vivo* fate [56, 57]. Therefore, the stability of liposomes against protein adsorption was evaluated by monitoring their particle size change in

the presence of serum. The particle size of cLip dramatically increased but that of PEGylated liposomes with or without preS1/21-47^{myr} modification remained unchanged in the presence of serum for 24 h (Fig. 4B). Hydrophilic PEG chains presented a large volume of hydrated layer on the liposome surface. Thus, the PEGylated liposmes showed increased colloidal stability than non-PEGylated liposomes in the presence of serum due to the steric repulsion by PEG chains against protein adsorption and electrostatic repulsion of the hydrated layer [58].

3.2 Cellular uptake

The preS1(21-47) region plays a critical role in the virus-cell interaction which can specifically bind with cell surface receptors on HepG2 [37, 39]. Also, more distinct binding was reported between preS1/21-47 and differentiated HepG2 induced by DMSO [46]. Thus, HepG2 and differentiated HepG2 cells were selected for the *in vitro* cellular uptake study. The uptake of preS1/21-47^{myr}-PEG-Lip was increased significantly compared to that of PEG-Lip in HepG2 cells ($P < 0.01$). Moreover, there was further improvement for the uptake of preS1/21-47^{myr}-PEG-Lip in the differentiated HepG2 cells while the uptake of PEG-Lip remained unchanged compared with HepG2 cells (Fig. 5A). In A549 cells, the uptake of preS1/21-47^{myr}-PEG-Lip increased significantly ($P < 0.05$) compared to that of PEG-Lip, however, no significant differences were observed for the uptake of preS1/21-47^{myr}-PEG-Lip in A549 cells and differentiated A549 cells. Despite the increase in the uptake of preS1/21-47^{myr}-PEG-Lip in HepG2 cells and A549 cells as compared to that of PEG-Lip, the uptake of the preS1/21-47^{myr}-PEG-Lip in HepG2 cells was inhibited by the pretreatment of free preS1/21-47^{myr} but not in A549 cells (Fig. 5B). Therefore, the increase in the uptake of preS1/21-47^{myr}-PEG-Lip in A549 and differentiated A549 cells could be attributed to the enhanced lipotropism induced

by the myristoyl acid residue of preS1/21-47^{myr}. In addition, the uptake of PEG-Lip in different cell types was not decreased by the free preS1/21-47^{myr}. The increase in the uptake of preS1/21-47^{myr}-PEG-Lip in HepG2 and differentiated HepG2 cells was demonstrated to be mediated by a ligand-receptor interaction and the enhanced lipotropism. After HepG2 differentiation, the uptake of preS1/21-47^{myr}-PEG-Lip was greatly improved, because the differentiated HepG2 cells displayed higher affinity to preS1/21-47 than HepG2 cells [46]. Moreover, the uptake of preS1/21-47^{myr}-PEG-Lip in the primary mice hepatocytes was dramatically improved compared with that of PEG-Lip and inhibited by free preS1/21-47^{myr} (Fig. 5A and Fig. 5B). Thus, the uptake of preS1/21-47^{myr}-PEG-Lip in the mice primary hepatocytes was suggested to be mediated by the ligand-receptor interaction. The obtained results were consistent with the literature, which suggested that HBV hepatotropism was mediated by a specific receptor recognition in the mice liver, and that the mice liver was not susceptible to HBV infection but expressed the HBV-preS1-specific receptors [34]. However, the identity of HBV-preS1-specific receptor remains unknown until now. Recently, sodium taurocholate cotransporting polypeptide (NTCP) was reported to function as a cellular receptor for viral entry of HBV through specific interaction between NTCP and the preS1 domain of HBV large envelope protein [59]. Therefore, NTCP may also be the corresponding receptor for preS1/21-47^{myr}, which remains to be addressed in the further study.

To determine the subcellular localization of liposomes, the cells were observed by the confocal laser scanning microscopy after being incubated in the medium containing Did-labeled liposomes for 1 h. The cell nuclei were stained with DAPI. As shown in Fig. 6, liposomes were mainly localized in the cytoplasm. In addition, the fluorescence of cLip and preS1/21-47^{myr}-PEG-Lip groups in cells were stronger than

that of PEG-Lip group. The images of preS1/21-47^{myr}-PEG-Lip group even displayed more fluorescence signal compared with that of cLip in differentiated HepG2 and mice primary hepatocytes. The results were in accordance with the data of flow cytometry analyses and confirmed the *in vitro* hepatic targetability of preS1/21-47^{myr}-PEG-Lip.

3.3 Cellular uptake pathway

To explore the endocytosis pathways for preS1/21-47^{myr} modified liposomes, the cellular uptake inhibition assay was adopted in liver cells including HepG2, differentiated HepG2 and mice primary hepatocytes. In this study, the cytotoxicity of different endocytosis inhibitors on HepG2, differentiated HepG2 and mice primary hepatocytes was negligible according to the MTT results (data not shown). Sodium azide was employed to determine the impact of energy. Colchicine, filipin and chlorpromazine were used to block macropinocytosis-mediated, caveolin-mediated and clathrin-mediated endocytosis, respectively [42, 60]. As shown in Fig. 7, the cellular uptake of preS1/21-47^{myr}-PEG-Lip was inhibited by sodium azide in all liver cells under investigation which indicated the endocytosis of preS1/21-47^{myr}-PEG-Lip was an energy-dependent process. The endocytosis pathways of conventional liposomes were proved to be mainly mediated by the clathrin-mediated endocytosis [61]. and fashioned by the peptide or the ligand exposed on the liposomes [62, 63]. In Fig. 7, the influence of colchicine was negligible which illustrated that minimal macropinocytosis effect in liver cells was observed for the internalization of preS1/21-47^{myr}-PEG-Lip. The chlorpromazine and filipin showed different effects on the cellular uptake of preS1/21-47^{myr}-PEG-Lip in three cell types. In HepG2, the cell uptake of preS1/21-47^{myr}-PEG-Lip was inhibited dramatically by chlorpromazine and slightly by filipin, which showed that the clathrin-mediated endocytosis played a

dominant role accompanied by the caveolin-mediated pathway. In the differentiated HepG2 cells and mice primary hepatocytes, the cell uptake of preS1/21-47^{myr}-PEG-Lip, on the contrary, was inhibited slightly by chlorpromazine and dramatically by filipin. Caveolae-mediated endocytosis is an important pathway for the cell entry of nanomedicine, which could bypass lysosomal degradation in most cases [62, 64]. Some viruses [65, 66] and macromolecules, such as albumin [67], exploited this pathway to prevent being degraded by lysosomes. Furthermore, HBV could enter cells via caveolin-mediated endocytosis [68, 69]. Thus, the preS1/21-47^{myr} derived from the large envelope protein of HBV may be endowed with the infection machinery of HBV, and as a result, the preS1/21-47^{myr}-PEG-Lip could enter liver cells by caveolin-mediated pathway and the caveolae-mediated endocytosis became stronger with higher affinity of preS1/21-47^{myr}-PEG-Lip to cells (HepG2 < differentiated HepG2 < primary hepatocytes).

3.4 *In vitro* cytotoxicity study

Consisting of a lipid bilayer which simulates the composition and structure of cell membrane, liposomes are thus generally well tolerated with low cytotoxicity [70, 71]. The cytotoxicity of the liposomes depends on the type of lipids, the amount of lipids, and the size and surface properties of liposomes [48, 72]. PreS1/21-47^{myr}-PEG-Lip and PEG-Lip did not induce significant cell cytotoxicity at various concentrations (up to 1 mg/mL) after incubation for 24 h and even lower cytotoxicity was observed with cLip at 1 mg/mL ($P < 0.05$) (Fig. 8). Therefore, the preS1/21-47^{myr}-PEG-Lip prepared in this study was proven a promising drug delivery system without obvious cytotoxicity.

3.5 *In vivo* biodistribution

To determine the *in vivo* liver targetability of preS1/21-47^{myr}-PEG-Lip, we next explored the biodistribution of Did-labeled preS1/21-47^{myr}-PEG-Lip in H22 tumor-bearing mice following intravenous administration. As shown in Fig. 9A and Fig. 9B, cLip were largely captured by the liver. After PEGylation, the uptake of liposomes was decreased markedly in liver and slightly in spleen. Meanwhile, the PEG-Lip remained mainly in the blood and was uptaken by tumor due to the enhanced permeability and retention effect (EPR effect) [73, 74]. After modification with preS1/21-47^{myr}, the preS1/21-47^{myr}-PEG-Lip displayed much higher liver concentration than that of PEG-Lip and of cLip ($P < 0.01$). In addition, the distribution of preS1/21-47^{myr}-PEG-Lip in tumor was slightly higher than that of PEG-Lip ($P < 0.05$), which was attributed to the dual impact of EPR effect and the active targeting of preS1/21-47^{myr}. Compared with cLip, the intratumoral distribution of preS1/21-47^{myr}-PEG-Lip increased dramatically in H22 tumor ($P < 0.01$).

The spleen capture of preS1/21-47^{myr}-PEG-Lip was slightly higher than PEG-Lip and similar with that of cLip (Fig. 9A and Fig. 9B), which might be owing to the modification of PEG-Lip surface property by preS1/21-47^{myr} with a myristoyl acid residue. Thus, it is necessary to determine the liver capture pathway of preS1/21-47^{myr}-PEG-Lip. As cLip was mainly captured by the Kuffer cells in liver not hepatocytes [2, 75], primary hepatocytes were isolated from mice liver to quantitatively determine the Did concentration by FCM. As shown in Fig. 9B and Fig. 9C, the uptake of cLip by hepatocytes was slightly higher than that of PEG-Lip though the uptake of cLip by whole liver was much higher than that of PEG-Lip. In contrast, the capture of preS1/21-47^{myr}-PEG-Lip by hepatocytes was in consistent with that by whole liver compared with PEG-Lip. Therefore, the capture of preS1/21-47^{myr}-PEG-Lip by liver was mainly mediated through the active targeting

process. In addition, hepatocytes account for more than 80% of the total resident hepatic cells and act as the most relevant target cells for liver diseases such as steatohepatitis, hepatocellular carcinoma, lantitrypsin deficiency and several other metabolic disorders [2]. Therefore, improving preS1/21-47^{myr}-PEG-Lip uptake by hepatocytes would be of great significance to liver targeted therapy.

3.6 *In vivo* antitumor efficacy

To study the antitumor efficacy of PTX-loaded preS1/21-47^{myr}-PEG-Lip on liver cancer, H22 transplanted tumor bearing ICR mice were chose as the model animals, which is a simple and fast-growing tumor model with high successful rate. After treatment with PTX injection and PTX-loaded liposomes, the tumor volumes and survival rates of mice were examined. As shown in Fig. 10, the tumor volumes increased rapidly in the saline group (mean tumor volume was 2897.45 mm^3 at the 19th day). It shows the variation of tumor volume with time (day) after H22 bearing mice were treated by *i.v.* of PTX injection, cLip-PTX and PEG-Lip-PTX and preS1/21-47^{myr}-PEG-Lip-PTX, respectively. Obviously, the mice treated with preS1/21-47^{myr}-PEG-Lip-PTX showed the slowest tumor growth rates and smallest tumor volumes, indicating that preS1/21-47^{myr}-PEG-Lip-PTX had the significant tumor inhibition ($P < 0.01$ versus saline, PTX injection and cLip-PTX treated groups and $P < 0.05$ versus PEG-Lip treated group). The effects of each treatment group on animal survival was displayed in Fig. 10 and Table 2 . The median survival of mice treated with preS1/21-47^{myr}-PEG-Lip-PTX (32 days) was significantly longer than that treated with saline (20 days, $P < 0.01$), PTX injection (22 days, $P < 0.01$), cLip-PTX (24 days, $P < 0.01$) and PEG-Lip-PTX (28 days, $P < 0.05$). Thus, it is clear that the antitumor efficacy of PTX *in vivo* was dramaticlly enhanced and the survival rates of tumor bearing mice were significantly improved by using the

hepatocyte-selective carrier system. In addition, preS1/21-47 is a strong entry inhibitor for the HBV infection [40], and the delivery system based on the peptide could improve the liver accumulation of drugs. Therefore, the carrier system also owns great potential in the therapy of the HBV infection.

3.7 *In vivo* safety evaluation

As discussed in the *in vitro* cytotoxicity study, the preS1/21-47^{myr}-PEG-Lip showed minimum toxicity for hepatogenic cells. To determine the *in vivo* safety, we further explored the general toxicity and immunotoxicity of preS1/21-47^{myr}-PEG-Lip. In the general toxicity study, no death and no serious body weight loss were observed compared with the saline group during the investigation period (Fig. 11A). No significant changes of hematologic and biochemical parameters were observed after the intravenous administration of blank preS1/21-47^{myr}-PEG-Lip for 2 weeks (Table 3 and Table 4). The serum levels of AST, ALT and ALP, as liver toxicity markers [76], remained unchanged by the repeated injection of blank preS1/21-47^{myr}-PEG-Lip, which indicated that there was no damage on hepatic cells though preS1/21-47^{myr}-PEG-Lip could distribute specifically in liver. In addition, no pathological changes were observed from histologic sections by administration of preS1/21-47^{myr}-PEG-Lip for 14-days (Fig. 11B), which demonstrated minimum organ toxicity after multiple administration of preS1/21-47^{myr}-PEG-Lip in 2 weeks.

IL-6 and IL-12 were selected as the cytokine markers to determine the systemic immunogenicity of the preS1/21-47^{myr}-PEG-Lip. As shown in Table 5, the serum levels of IL-6 and IL-12 in mice were greatly increased after being administrated with LPS. However, no significant differences for inflammatory cytokine levels were observed in serum between the preS1/21-47^{myr}-PEG-Lip group and saline group.

These results demonstrated that preS1/21-47^{myr}-PEG-Lip did not induce significant immune response of mice after injection.

4. Conclusions

In this work, we have demonstrated the successful application of N-myristoyl preS1/21-47 to prepare a liver targeted drug delivery system with high specificity to hepatogenic cells. The preS1/21-47^{myr}-PEG-Lip showed outstanding targetability to hepatic cells including hepatoma carcinoma cells *in vitro* and *in vivo*. In addition, preS1/21-47^{myr}-PEG-Lip did not induce acute systemic toxicity and immunogenicity or induce hepatotoxicity *in vivo*. Taken together, preS1/21-47^{myr}-PEG-Lip represents an effective and safe delivery system for targeted liver disease therapy and imaging.

Acknowledgments

The work was supported by the National Natural Science Foundation of China (81273443), the National S&T Major Project of China (2012ZX09304004) and the National Basic Research Program of China (2013CB932504).

References

1. L. Li, H. Wang, Z. Y. Ong, K. Xu, P. L. R. Ee, S. Zheng, J. L. Hedrick and Y.-Y. Yang, *Nano Today*, 2010, 5, 296-312.
2. K. Poelstra, J. Prakash and L. Beljaars, *J. Control. Release*, 2012, 161, 188-197.
3. J.-H. Kang, J. Oishi, J.-H. Kim, M. Ijuin, R. Toita, B. Jun, D. Asai, T. Mori, T. Niidome and K. Tanizawa, *Nanomed.-Nanotechnol.*, 2010, 6, 583-589.
4. D. E. Owens III and N. A. Peppas, *Int. J. Pharm.*, 2006, 307, 93-102.
5. Z. Panagi, A. Beletsi, G. Evangelatos, E. Livaniou, D. Ithakissios and K. Avgoustakis, *Int. J. Pharm.*, 2001, 221, 143-152.
6. L. Fiume, L. Bolondi, C. Busi, P. Chieco, F. Kratz, M. Lanza, A. Mattioli and G. Di Stefano, *J. Hepatol.*, 2005, 43, 645-652.
7. D.-Q. Wu, B. Lu, C. Chang, C.-S. Chen, T. Wang, Y.-Y. Zhang, S.-X. Cheng, X.-J. Jiang, X.-Z. Zhang and R.-X. Zhuo, *Biomaterials*, 2009, 30, 1363-1371.
8. L. Beljaars, G. Molema, B. Weert, H. Bonnema, P. Olinga, G. M. Groothuis, D. K. Meijer and K. Poelstra, *Hepatology*, 1999, 29, 1486-1493.
9. K. Hirata, T. Maruyama, H. Watanabe, H. Maeda, K. Nakajou, Y. Iwao, Y. Ishima, H. Katsumi, M. Hashida and M. Otagiri, *J. Control. Release*, 2010, 145, 9-16.
10. Q. Tian, C.-N. Zhang, X.-H. Wang, W. Wang, W. Huang, R.-T. Cha, C.-H. Wang, Z. Yuan, M. Liu and H.-Y. Wan, *Biomaterials*, 2010, 31, 4748-4756.
11. C. Zhang, W. Wang, T. Liu, Y. Wu, H. Guo, P. Wang, Q. Tian, Y. Wang and Z. Yuan, *Biomaterials*, 2012, 33, 2187-2196.
12. W. H. Kong, K. Park, M.-Y. Lee, H. Lee, D. K. Sung and S. K. Hahn, *Biomaterials*, 2013, 34, 542-551.
13. P. C. Rensen, R. L. de Vrueh, J. Kuiper, M. K. Bijsterbosch, E. A. Biessen and T. J. van Berkel, *Adv. Drug Delivery Rev.*, 2001, 47, 251-276.
14. Y. Takakura, S. Masuda, H. Tokuda, M. Nishikawa and M. Hashida, *Biochem. Pharmacol.*, 1994, 47, 853-858.
15. F. Umezawa and Y. Eto, *Biochem. Bioph. Res. Co.*, 1988, 153, 1038-1044.
16. S. Zhu, M. Niu, H. O'Mary and Z. Cui, *Mol. Pharm.*, 2013, 10, 3525-3530.
17. H. J. Haisma and A. R. Bellu, *Mol. Pharm.*, 2010, 8, 50-55.
18. R. Hong, W. Bai, J. Zhai, W. Liu, X. Li, J. Zhang, X. Cui, X. Zhao, X. Ye and Q. Deng, *J. Virol.*, 2013, 87, 6615-6624.
19. U. Protzer, M. Nassal, P.-W. Chiang, M. Kirschfink and H. Schaller, *Proc. Natl. Acad. Sci. USA*, 1999, 96, 10818-10823.
20. J. Yoo, J. Rho, D. Lee, S. Shin and G. Jung, *Virus genes*, 2002, 24, 215-224.
21. M. Yamada, A. Oeda, J. Jung, M. Iijima, N. Yoshimoto, T. Niimi, S.-Y. Jeong, E. K. Choi, K. Tanizawa and S. i. Kuroda, *J. Control. Release*, 2012, 160, 322-329.
22. T. Yamada, Y. Iwasaki, H. Tada, H. Iwabuki, M. K. Chuah, T. VandenDriessche, H. Fukuda, A. Kondo, M. Ueda and M. Seno, *Nat. Biotechnol.*, 2003, 21, 885-890.
23. J. Jung, T. Matsuzaki, K. Tatematsu, T. Okajima, K. Tanizawa and S. i. Kuroda, *J. Control. Release*, 2008, 126, 255-264.
24. K. Khatri, A. Rawat, S. Mahor, P. N. Gupta and S. P. Vyas, *J. Drug Target.*, 2005, 13, 359-366.
25. M. Giacca and S. Zacchigna, *J. Control. Release*, 2012, 161, 377-388.

26. A. Barrera, B. Guerra, L. Notvall and R. E. Lanford, *J. Virol.*, 2005, 79, 9786-9798.
27. W. Mier, A. Schieck, A. Schulze, U. Haberkorn, A. Alexandrov and S. Urban, 2012.
28. D. Glebe, *World J. Gastroenterol.*, 2007, 13, 65-73.
29. D. Glebe, M. Aliakbari, P. Krass, E. V. Knoop, K. P. Valerius and W. H. Gerlich, *J. Virol.*, 2003, 77, 9511-9521.
30. P. Gripon, I. Cannie and S. Urban, *J. Virol.*, 2005, 79, 1613-1622.
31. P. Gripon, J. Le Seyec, S. Rumin and C. Guguen-Guillouzo, *Virology*, 1995, 213, 292-299.
32. A. Schulze, P. Gripon and S. Urban, *Hepatology*, 2007, 46, 1759-1768.
33. J. Petersen, M. Dandri, W. Mier, M. Lütgehetmann, T. Volz, F. von Weizsäcker, U. Haberkorn, L. Fischer, J.-M. Pollok and B. Erbes, *Nat. Biotechnol.*, 2008, 26, 335-341.
34. A. Schieck, A. Schulze, C. Gähler, T. Müller, U. Haberkorn, A. Alexandrov, S. Urban and W. Mier, *Hepatology*, 2013, 58, 43-53.
35. X. Zhang, Q. Zhang, Q. Peng, J. Zhou, L. Liao, X. Sun, L. Zhang and T. Gong, *Biomaterials*, 2014, 35, 6130-6141.
36. A. Meier, S. Mehrle, T. S. Weiss, W. Mier and S. Urban, *Hepatology*, 2013, 58, 31-42.
37. S. Dash, K. V. Rao and S. K. Panda, *Journal of medical virology*, 1992, 37, 116-121.
38. A. Neurath, S. Kent, N. Strick and K. Parker, *Cell*, 1986, 46, 429-436.
39. M.-A. Petit, S. Dubanchet, F. Capel, P. Voet, C. Dauguetj and P. Hausert, *Virology*, 1991, 180, 483-491.
40. M. Murata, S. Narahara, K. Umezaki, R. Toita, S. Tabata, J. S. Piao, K. Abe, J.-H. Kang, K. Ohuchida and L. Cui, *International journal of nanomedicine*, 2012, 7, 4353.
41. N. Paran, A. Cooper and Y. Shaul, *Rev. Med. Virol.*, 2003, 13, 137-143.
42. Q. Zhang, J. Tang, L. Fu, R. Ran, Y. Liu, M. Yuan and Q. He, *Biomaterials*, 2013, 34, 7980-7993.
43. H. Schägger, *Nat. Protoc.*, 2006, 1, 16-22.
44. X. Sun, Z. Pang, H. Ye, B. Qiu, L. Guo, J. Li, J. Ren, Y. Qian, Q. Zhang and J. Chen, *Biomaterials*, 2012, 33, 916-924.
45. H.-X. Wang, M.-H. Xiong, Y.-C. Wang, J. Zhu and J. Wang, *J. Control. Release*, 2013, 166, 106-114.
46. N. Paran, B. Geiger and Y. Shaul, *The EMBO journal*, 2001, 20, 4443-4453.
47. S. Ouasti, P. J. Kingham, G. Terenghi and N. Tirelli, *Biomaterials*, 2012, 33, 1120-1134.
48. J.-H. Park, H.-J. Cho, H. Y. Yoon, I.-S. Yoon, S.-H. Ko, J.-S. Shim, J.-H. Cho, J. H. Park, K. Kim and I. C. Kwon, *J. Control. Release*, 2014, 174, 98-108.
49. Z. Zhu, Y. Li, X. Li, R. Li, Z. Jia, B. Liu, W. Guo, W. Wu and X. Jiang, *J. Control. Release*, 2010, 142, 438-446.
50. E. Kinkead, R. Wolfe, S. Salins, C. Flemming, H. Leahy, D. Caldwell, C. Miller and G. Marit, *Toxicol. Ind. Health*, 1995, 11, 199-215.
51. J. Zhou, X. Zhang, M. Li, W. Wu, X. Sun, L. Zhang and T. Gong, *Mol. Pharm.*, 2013, 10, 3832-3841.
52. S. Chono, S.-D. Li, C. C. Conwell and L. Huang, *Journal of Controlled Release*, 2008, 131, 64-69.

53. N. Savaraj, L. G. Feun, K. Lu, K. Gray, C. Wang and T. L. Loo, *J. Neurooncol.*, 1992, 13, 211-215.
54. S. De Falco, M. Ruvo, A. Verdoliva, A. Scarallo, D. Raimondo, A. Raucci and G. Fassina, *J. Pept. Res.*, 2001, 57, 390-400.
55. M. Elmowafy, T. Viitala, H. M. Ibrahim, S. K. Abu-Elyazid, A. Samy, A. Kassem and M. Yliperttula, *Eur. J. Pharm. Sci.*, 2013, 50, 161-171.
56. F. Alexis, E. Pridgen, L. K. Molnar and O. C. Farokhzad, *Mol. Pharm.*, 2008, 5, 505-515.
57. R. Müller and K. H. Wallis, *Int. J. Pharm.*, 1993, 89, 25-31.
58. L. N. Ramana, S. Sharma, S. Sethuraman, U. Ranga and U. M. Krishnan, *Int. J. Pharm.*, 2012, 431, 120-129.
59. H. Yan, G. Zhong, G. Xu, W. He, Z. Jing, Z. Gao, Y. Huang, Y. Qi, B. Peng and H. Wang, *elife*, 2012, 1.
60. K. Xiao, Y. Li, J. Luo, J. S. Lee, W. Xiao, A. M. Gonik, R. G. Agarwal and K. S. Lam, *Biomaterials*, 2011, 32, 3435-3446.
61. K. Un, K. Sakai-Kato, Y. Oshima, T. Kawanishi and H. Okuda, *Biomaterials*, 2012, 33, 8131-8141.
62. D. Mudhakir, H. Akita, E. Tan and H. Harashima, *J. Control. Release*, 2008, 125, 164-173.
63. Y. Zhang, X. Rong Qi, Y. Gao, L. Wei, Y. Maitani and T. Nagai, *J. Control. Release*, 2007, 117, 281-290.
64. G. Sahay, D. Y. Alakhova and A. V. Kabanov, *J. Control. Release*, 2010, 145, 182-195.
65. L. Pelkmans, *BBA-Mol. Cell Res.*, 2005, 1746, 295-304.
66. L. Pelkmans, J. Kartenbeck and A. Helenius, *Nat. Cell Biol.*, 2001, 3, 473-483.
67. J. E. Schnitzer and P. Oh, *J. Biol. Chem.*, 1994, 269, 6072-6082.
68. X. Hao, X. Shang, J. Wu, Y. Shan, M. Cai, J. Jiang, Z. Huang, Z. Tang and H. Wang, *small*, 2011, 7, 1212-1218.
69. A. Macovei, C. Radulescu, C. Lazar, S. Petrescu, D. Durantel, R. A. Dwek, N. Zitzmann and N. B. Nichita, *J. Virol.*, 2010, 84, 243-253.
70. E. Mayhew, M. Ito and R. Lazo, *Exp. Cell Res.*, 1987, 171, 195-202.
71. M. Slingerland, H.-J. Guchelaar and H. Gelderblom, *Drug Discov. Today*, 2012, 17, 160-166.
72. R. Zeisig, K. Müller, N. Maurer, D. Arndt and A. Fahr, *J. Membr. Biol.*, 2001, 182, 61-69.
73. M. J. Ernsting, W. D. Foltz, E. Undzys, T. Tagami and S.-D. Li, *Biomaterials*, 2012, 33, 3931-3941.
74. K. Takara, H. Hatakeyama, G. Kibria, N. Ohga, K. Hida and H. Harashima, *J. Control. Release*, 2012, 162, 225-232.
75. T. Daemen, M. Velinova, J. Regts, M. de Jager, R. Kalicharan, J. Donga, J. Van Der Want and G. L. Scherphof, *Hepatology*, 1997, 26, 416-423.
76. J. S. Ozer, R. Chetty, G. Kenna, J. Palandra, Y. Zhang, A. Lanevschi, N. Koppiker, B. E. Souberbielle and S. K. Ramaiah, *Regul. Toxicol. Pharmacol.*, 2010, 56, 237-246.

Table 1 Characrteristics of cLip, PEG-Lip and preS1/21-47^{myr}-PEG-Lip (n = 3, mean ± SD).

Code	Particle size (nm)	Polydispersity	ζ (mV)	Encapsulation efficiency (%)
Blank liposomes				
PEG-Lip	115.3 ± 5.5	0.126 ± 0.009	-10.4 ± 2.0	
PreS1/21-47^{myr}-PEG-Lip	133.6 ± 10.3	0.202 ± 0.015	-11.7 ± 1.3	
cLip	157.6 ± 8.4	0.275 ± 0.022	-8.5 ± 1.6	
PTX loaded liposomes				
PEG-Lip	126.6 ± 4.1	0.152 ± 0.014	-8.2 ± 1.4	96.5 ± 2.4
PreS1/21-47^{myr}-PEG-Lip	141.2 ± 5.2	0.246 ± 0.029	-10.5 ± 3.6	93.4 ± 3.1
cLip	167.3 ± 6.4	0.278 ± 0.041	-9.6 ± 2.1	91.5 ± 3.7

Table 2 Effect of PTX formulations on survival time of the xenografted hepatoma H22-burding mice.

Groups	Survival time (days)		Compare with			
	Means	Medians	Saline	PTX injection	cLip-PTX	PEG-Lip-PTX
Saline	19.5 ± 0.8	20.0 ± 1.1	_	_	_	_
PTX injection	21.5 ± 0.9	22.0 ± 1.1	N.S.	_	_	_
cLip-PTX	24.3 ± 1.0	24.0 ± 1.1	**	*	_	_
PEG-Lip-PTX	27.7 ± 1.2	28.0 ± 1.1	**	**	*	_
preS1/21-47^{myr}-PEG-Lip-PTX	33.0 ± 1.8	32.0 ± 2.3	**	**	**	*

*** P < 0.05, ** P < 0.01, N.S. P > 0.05 of log-rank analysis.**

Table 3 Serum biochemical parameters of mice after intravenous saline or blank preS1/21-47^{myr}-PEG-Lip treatment for 2 weeks (mean ± SD, n = 6).

Parameters	Saline	Blank preS1/21-47^{myr}-PEG-Lip
AST (U/L)	137.2 ± 34.5	114.5 ± 27.4
ALT (U/L)	42.3 ± 15.7	47.9 ± 10.1
Total bilirubin (μmol/L)	1.7 ± 0.3	1.8 ± 0.4
ALP (U/L)	156.3 ± 41.7	141.2 ± 39.4
BUN (mmol/L)	6.1 ± 1.7	6.6 ± 1.2
CREA (μmol/L)	13.2 ± 5.2	11.8 ± 3.9
CK (U/L)	701.5 ± 119.4	721.4 ± 84.0

LDH (U/L)	517.6 ±102.4	594.3 ±151.8

Table 4 Hematology parameters of mice after intravenous saline or blank preS1/21-47^{myr}-PEG-Lip treatment for 2 weeks (mean ± SD, *n* = 6).

Parameters	Saline	Blank preS1/21-47^{myr}-PEG-Lip
WBC (10^9/L)	6.4 ±0.7	7.3 ±0.9
RBC (10^{12}/L)	8.5 ±0.4	9.2 ±0.5
Platelet (10^9/L)	607.8 ±62.7	664.6 ±137.4
Lymphs (%)	61.2 ±10.3	70.4 ±12.5
Hemoglobin (g/L)	158.9 ±10.7	137.1 ±8.1
Hematocrit (%)	43.2 ±4.6	49.5 ±7.4
MCV (fL)	50.3 ±4.1	45.4 ±2.9
MCH (pg)	14.5 ±0.8	15.8 ±2.4
MCHC (g/L)	255.4 ±52.9	239.0 ±24.5

Table 5 Serum IL-6 and IL-12 levels of mice executed 2 h after intravenous administration of saline, blank preS1/21-47^{myr}-PEG-Lip and LPS (mean ± SD, *n* = 6).

Cytokines	Saline	Blank preS1/21-47^{myr}-PEG-Lip	LPS
IL-6 (pg/mL)	30.2 ±8.2	32.5 ±6.9	452.4 ±179.9
IL-12 (pg/mL)	845.7 ±165.2	874.3 ±221.4	4926.1 ±2930.6

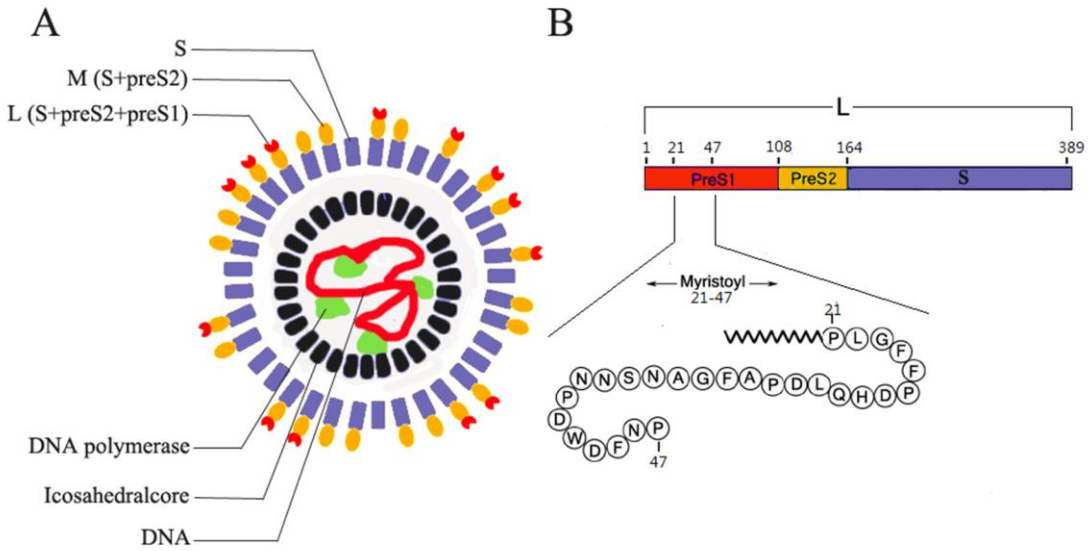

Fig. 1 (A) Schematic structure of HBV, which shows that the viral DNA covalently attached to the DNA polymerase and the complex is enclosed by an inner nucleocapsid and an outer envelope which containing three different surface proteins termed Small (S), Middle (M) and Large (L). (B) Schematic structure of the L surface protein of HBV with preS1 domain, preS2 domain, and S domain. The preS1/21-47^{myr} comprising the prominent HBV attachment epitope (amino acids 21–47 of the preS1 domain) with N-terminal myristoylation.

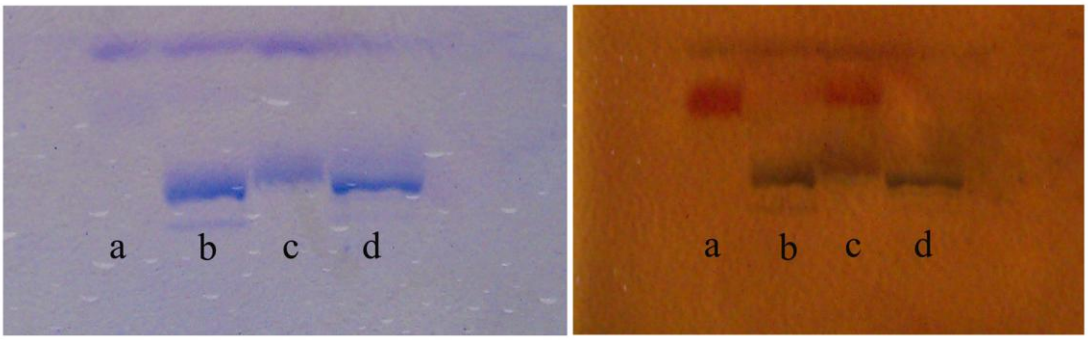

Fig. 2 Reaction of preS1/21-47^{myr} and Mal-PEG-DSPE as monitored by Tricine-SDS-PAGE. The gel was dyed with 0.25% of coomassie brilliant blue for detecting the preS1/21-47^{myr} (left) and then dyed by potassium iodide solution containing iodine for tracing the Mal-PEG$_{2000}$-DSPE (right). (a) Mal-PEG$_{2000}$-DSPE, (b) reaction solution of Mal-PEG$_{2000}$-DSPE and preS1/21-47^{myr} (excess), (c) reaction solution of Mal-PEG2000-DSPE (excess) and preS1/21-47^{myr}, (d) preS1/21-47^{myr}.

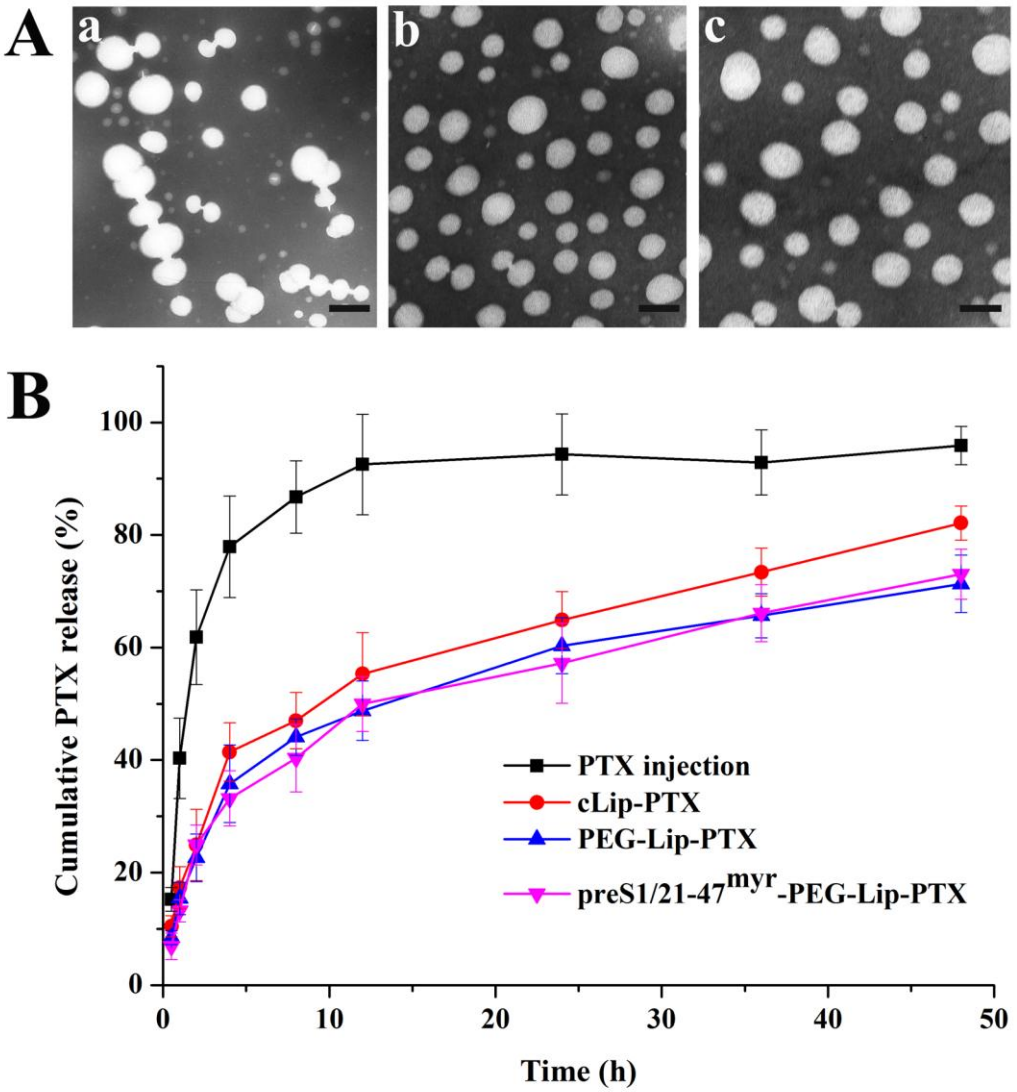

Fig. 3 (A) Transmission electron micrographs of PEG-Lip (a), preS1/21-47^{myr}-PEG-Lip (b) and cLip (c). The scale bar represents 100 nm. (B) The *in vitro* release profiles of PTX injection and PTX loaded liposomes (*n* = 3, mean ± SD).

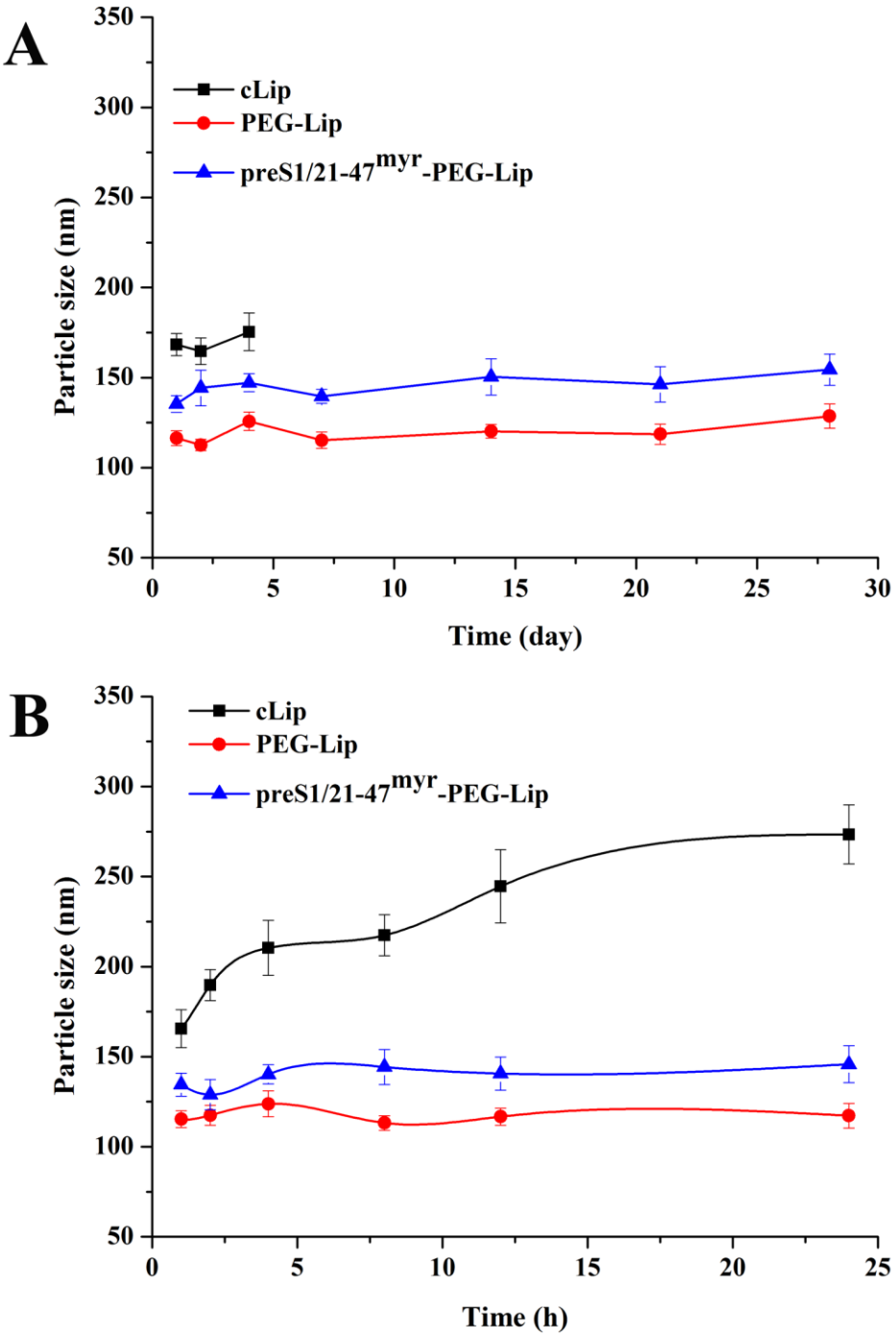

Fig. 4 Representative graphs of particle size of Did loaded cLip, PEG-Lip and preS1/21-47^{myr}-PEG-Lip at 4 ℃ (A) and in the presence of 50% FBS (B) (n = 3, mean ± SD).

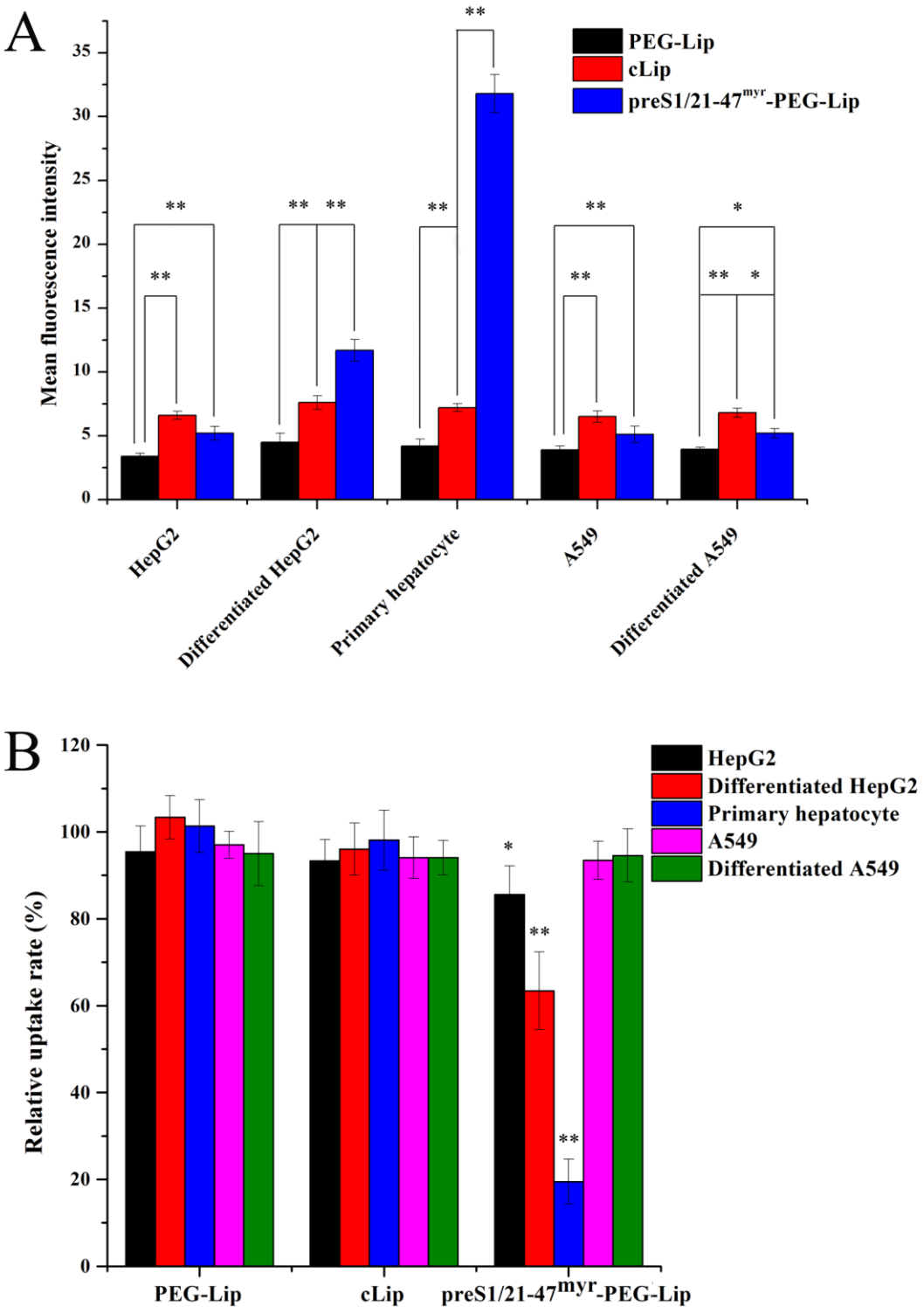

Fig. 5 FCM analysis of HepG2, differentiated HepG2, primary hepatocytes, A549 and differentiated A549 cells treated with Did loaded cLip, PEG-Lip and preS1/21-47^{myr}-PEG-Lip for 1 h at 37 ℃ in the absence (A) and the presence (B) of 25 μg/mL of preS1/21-47^{myr}, data represent mean ± SD (n = 3), * P < 0.05, ** P < 0.01 versus the uptake with the absence of preS1/21-47^{myr}.

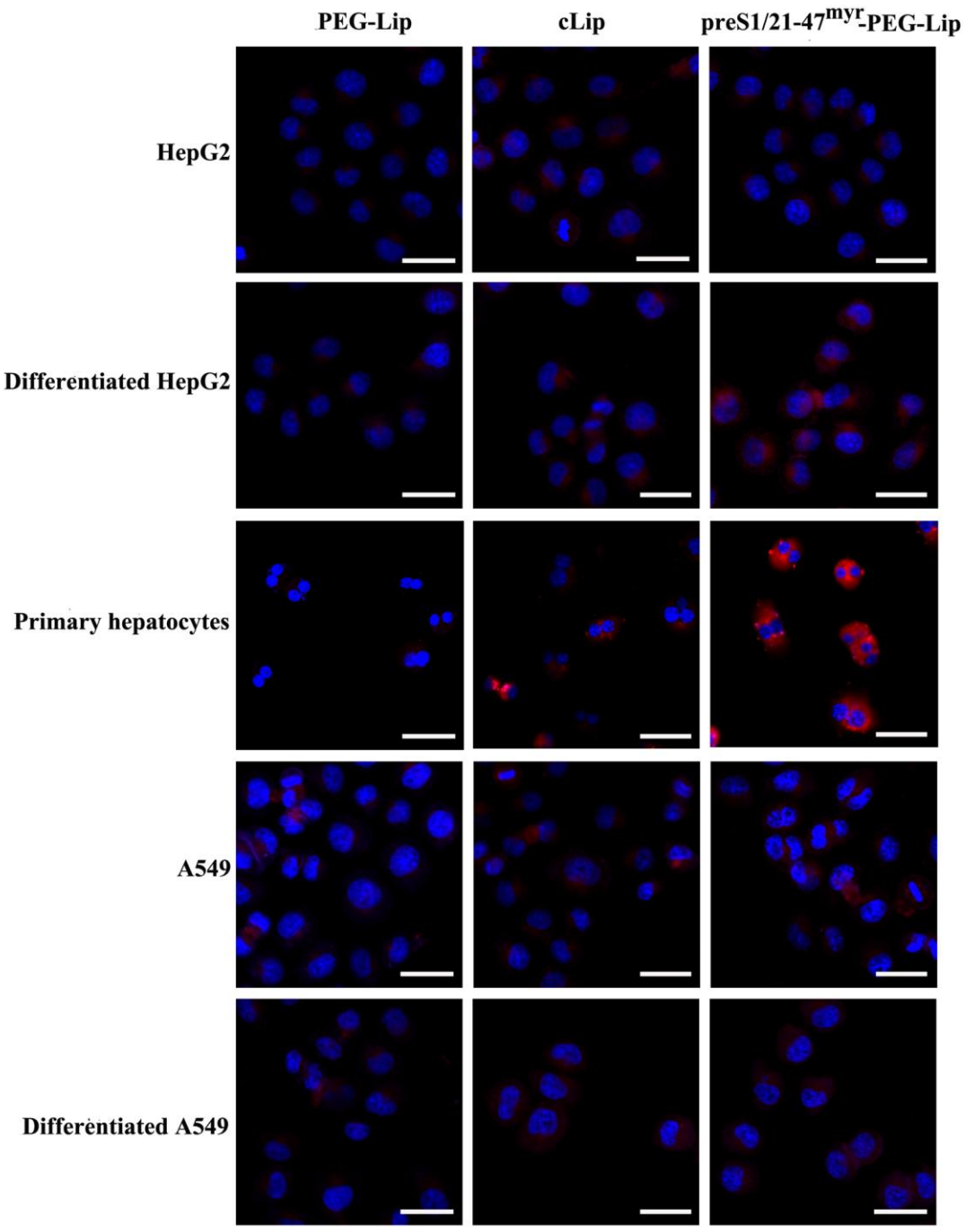

Fig. 6 Confocal microscopy images of HepG2, differentiated HepG2, primary hepatocytes, A549 and differentiated A549 incubated with Did-labeled PEG-Lip, cLip and preS1/21-47^{myr}-PEG-Lip for 1 h at 37 ℃. Red represents fluorescence of Did and blue represents fluorescence of DAPI. Scale bars represent 50 μm.

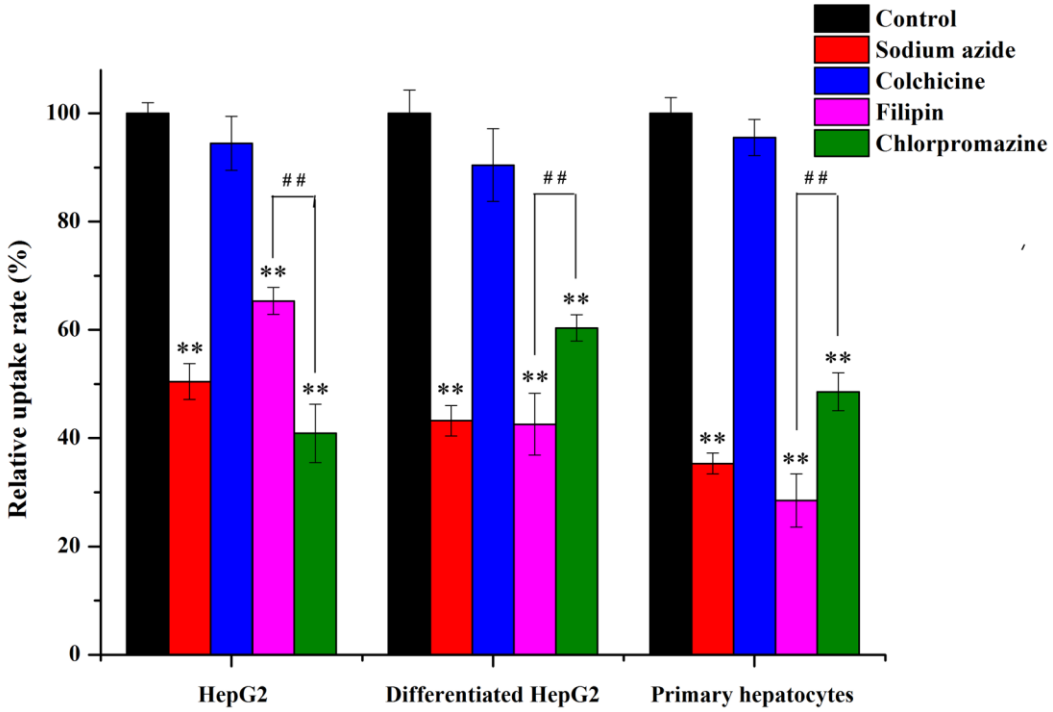

Fig. 7 The relative uptake percentage of preS1/21-47^{myr}-PEG-Lip on HepG2 cells, differentiated HepG2 cells and primary hepatocytes in the presence of endocytosis inhibitors including sodium azide, colchicine, filipin, and chloropromazine. Data were normalized to the control group with no endocytosis inhibitor treatment. Cells were pre-incubated with different inhibitors for 30 min and then treated with preS1/21-47^{myr}-PEG-Lip for another 1 h. Data represent mean ± SD (n = 3), ** P < 0.01 versus control, # # P < 0.01.

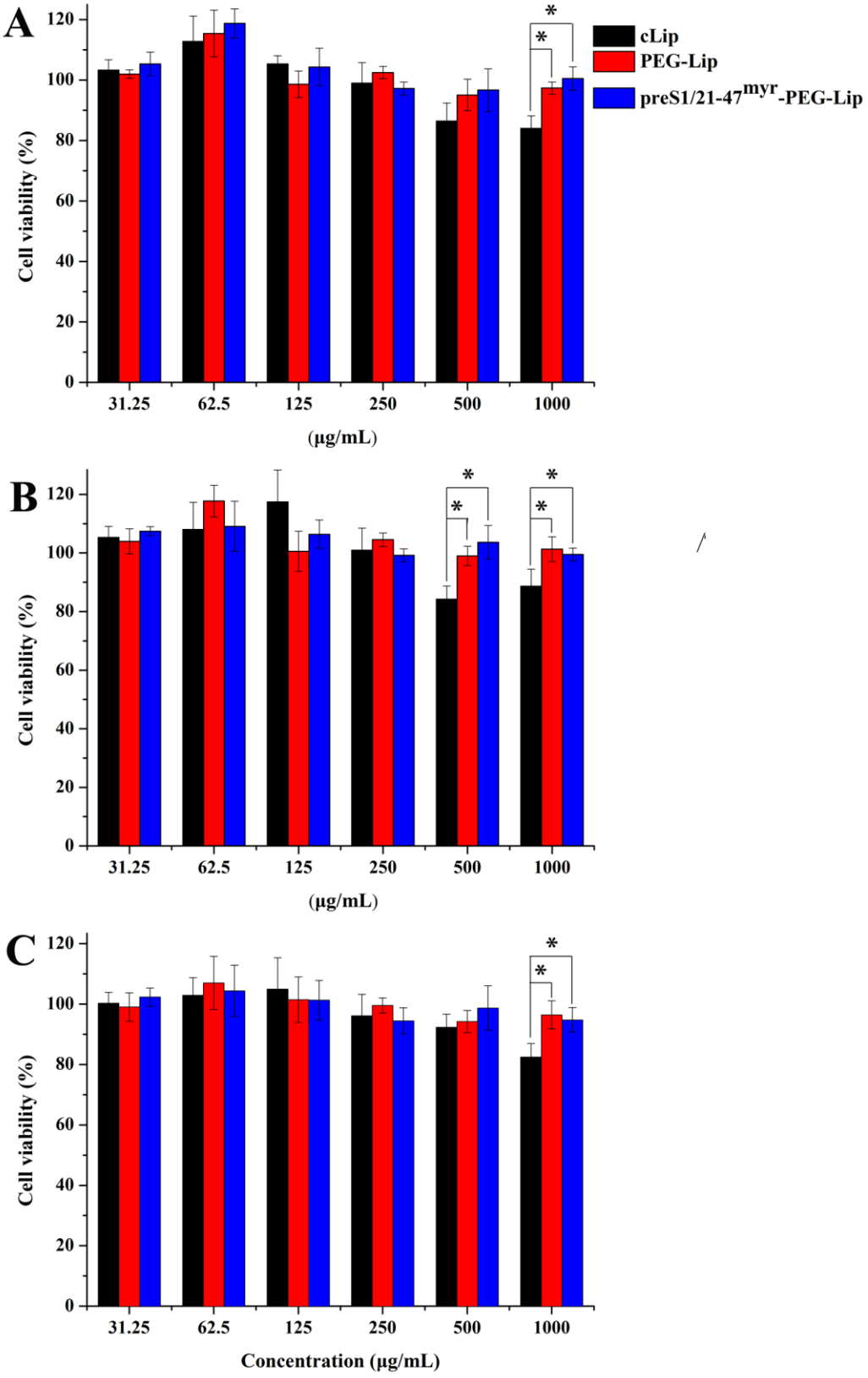

Fig. 8 *In vitro* cytotoxicity of blank cLip, PEG-Lip and preS1/21-47^{myr}-PEG-Lip in HepG2 cells (A), differentiated HepG2 cells (B) and primary hepatocytes (C). Blank cLip, PEG-Lip and preS1/21-47^{myr}-PEG-Lip (31.25 - 1000 μg/mL) were incubated with cells for 24 h. Cell viability (%) was measured using a MTT-based assay. Data represent mean ± SD (n = 3), * P < 0.05.

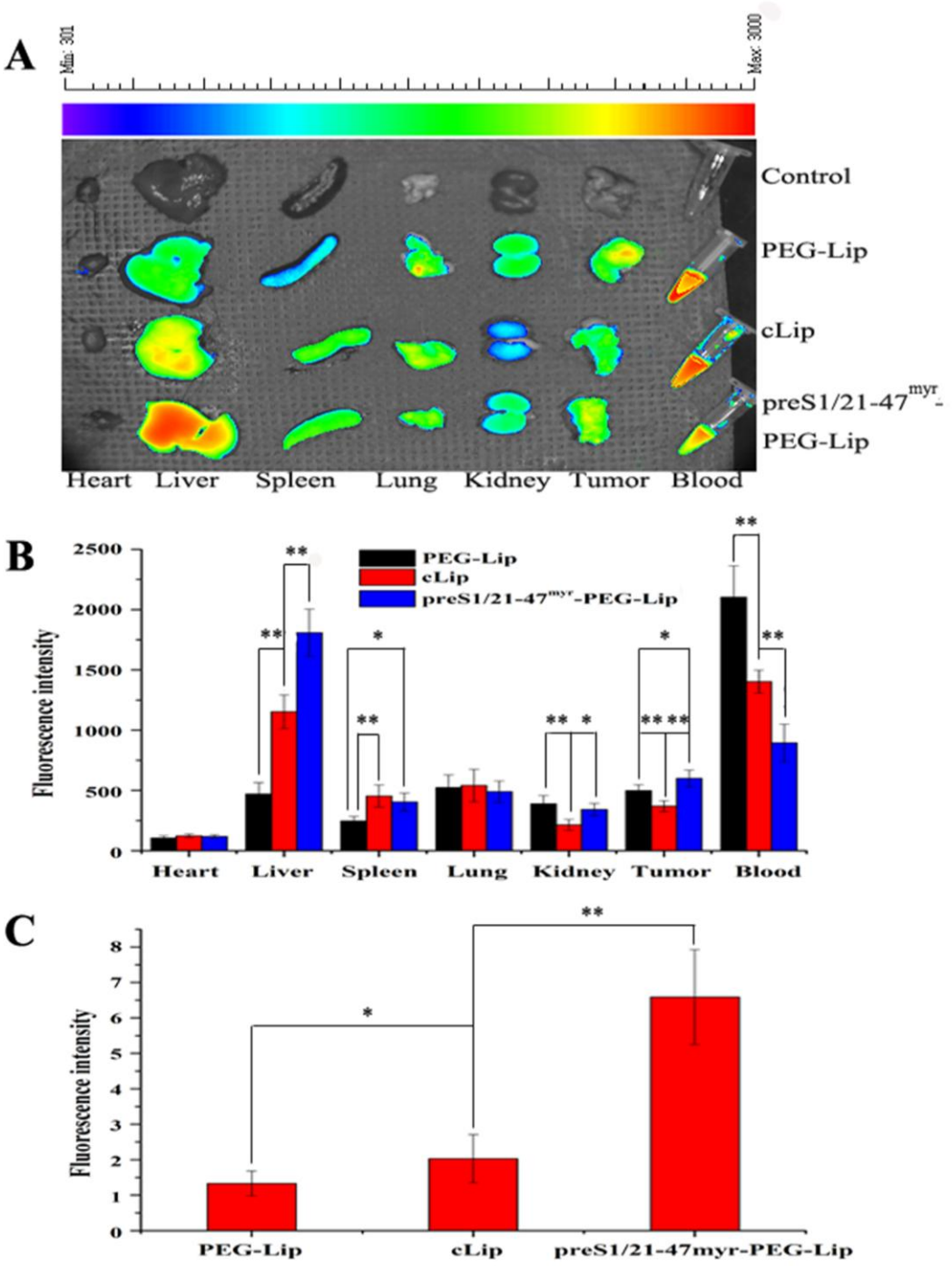

Fig. 9 (A) *Ex vivo* imaging of liposomes in main organs of ICR mice at 1h post-injection with Did labeled cLip, PEG-Lip and preS1/21-47^{myr}-PEG-Lip. (B) The statistical graphs of the fluorescence intensity of main organs and blood based on the semi-quantitative analysis of the *ex vivo* fluorescence images of mice attained at 1 h after *i.v.* administration of Did labeled liposomes. Data represent mean ± SD (n = 5), * P < 0.05, ** P < 0.01. (C) FCM analysis of Did in parenchymal hepatic cells from mice receiving Did labeled cLip, PEG-Lip and preS1/21-47^{myr}-PEG-Lip. Data represent mean ± SD (n = 5), * P < 0.05, ** P < 0.01.

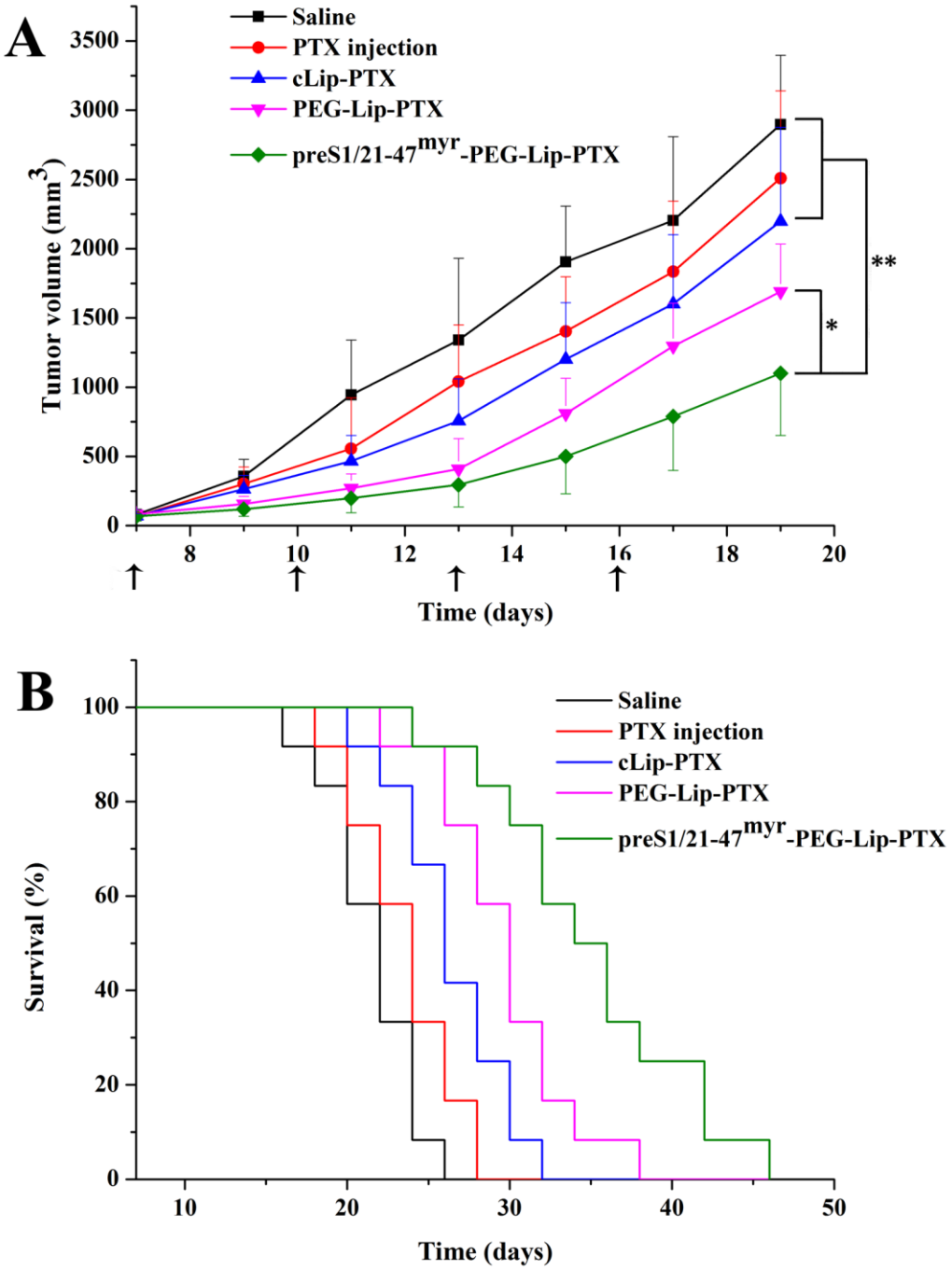

Fig. 10 *In vivo* tumor volumes (A) and Kaplan-Meier survival curves (B) of xenografted hepatoma H22-burding mice treated with saline, PTX injection, cLip-PTX, PEG-Lip-PTX and preS1/21-47^{myr}-PEG-Lip-PTX (PTX dose 5 mg/kg), respectively, at day 7, 10, 13 and 16 post implantation (n = 12). * $P < 0.05$, ** $P < 0.01$.

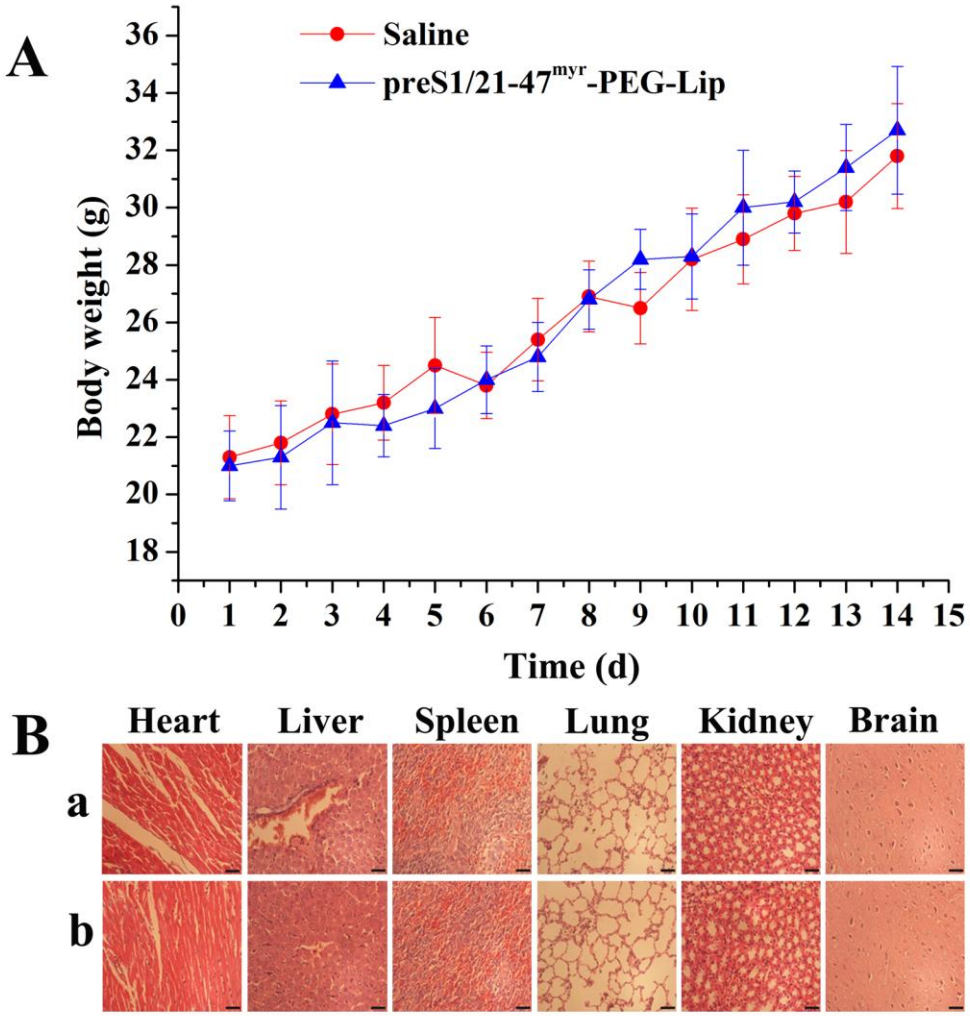

Fig. 11 (A) Body weight changes of ICR mice following daily treatment of saline or blank preS1/21-47^{myr}-PEG-Lip for 14 days. Data represent mean ± SD (n = 8). (B) Histological staining of main organs from ICR mice following 14 days treatment with saline and blank preS1/21-47^{myr}-PEG-Lip. Scale bars represent 125 μm.